Timepix3 detector for measuring radon decay products

Published by IOP Publishing for Sissa Medialab

Received: *December 21, 2021*
Revised: *February 22, 2022*
Accepted: *April 26, 2022*
Published: *June 7, 2022*

Timepix3 detector for measuring radon decay products

A. Tamburrino,[a,b,d,*] **G. Claps,**[a,b] **F. Cordella,**[a,b] **F. Murtas**[b,c] **and D. Pacella**[a,b]

[a] *ENEA Fusion and Nuclear Safety Department, C. R. Frascati, via E. Fermi 45, 00044 Frascati, Italy*
[b] *INFN — Laboratori Nazionali di Frascati, via E. Fermi 40, 00044 Frascati, Italy*
[c] *CERN, CH-1211 Geneva 23, Switzerland*
[d] *DIAEE-Dipartimento di Ingegneria Astronautica, Elettrica ed Energetica, Sapienza Università di Roma, Piazzale Aldo Moro 5, 00185 Roma, Italy*

E-mail: antonella.tamburrino@uniroma1.it

Abstract: The present work is focused on the characterization of a Timepix3 (TPX3) based test system for the identification of particles produced by the complex decay chain of ^{222}Rn. The detector used is composed of a pixelated Cadmium Telluride (CdTe) semiconductor (500 µm thick) bump-bonded on an ASIC TPX3 chip. Measurements were carried out at the NIXT Laboratory (ENEA Frascati) using radioactive sources and exploiting the presence of natural radon gas by collecting its decay products on the sensor surface. Estimation of the radon gas risk is one of the most important problems in radiation protection and has stimulated further development of new advanced methods suitable for detecting this gas in confined environments. A study of the spatial uniformity and high energy calibration is also presented and an improved cluster analysis is introduced. The performance highlighted in this study will allow a detailed and faster analysis of the radon products and may have an important impact on the environmental radioprotection applications. This paper describes the application and use of this test system to identify the different decay signatures and follow the temporal evolution of the Radon decay chain.

Keywords: Particle identification methods; Heavy-ion detectors; Timing detectors; Particle tracking detectors (Solid-state detectors)

*Corresponding author.

https://doi.org/10.1088/1748-0221/17/06/P06009

2022 JINST 17 P06009

Contents

2022 JINST 17 P06009

1 Introduction

For the whole course of its existence, a human being is exposed to radiation of natural origin. The set of all these radiation sources forms what is called the natural radiation background, and it is now widely recognized that the most significant component of exposure is the inhalation of radon decay products. Radon and its progeny constitute the preponderant share of man's overall exposure to ionizing radiation of natural origin. The Scientific Committee of the United Nations in the study of the effects of ionizing radiation has in fact estimated that indoor radon is responsible for 50% of the exposure dose due to ionizing radiation from natural sources (UNSCEAR2020) [1]. As a descendant of uranium, radon is constantly generated in the Earth's crust; uranium, in fact, is widely present in the soil and rocks and thus also in the building materials. The radon thus produced occurs in the air, but the concentration indoors is considerably higher than outdoors due to volume dilution. Being a noble gas, radon is not typically absorbed by the ground and, for this reason, it tends to filter upwards. Therefore, in a closed environment at the ground level, the concentration of radon tends to increase. Then, although not harmful in the open air, it can become a significant source of risk in indoor environments where it can be inhaled while breathing. In nature radon is present in three different isotopes: ^{222}Rn (radon), ^{220}Rn (thoron) and ^{219}Rn (actinon). Due to its half-life of 3.82 days, radon can reach distances up to several hundreds of meters relative to its place of origin. To a lesser degree, thoron can also reach inhabited areas because of its half-life of about 56 s, but it is present in lower concentrations. Actinon, instead, having a half-life time of few seconds and small concentrations does not make any contribution. For these reasons, attention is focused almost exclusively on ^{222}Rn. However, it is important to underline the fact that radon, as a noble gas, does not pose a risk because it is exhaled with little exposure of the respiratory tract to alpha particles. The risk is linked to the radioactive emissions of the radon progeny, such as ^{218}Po, ^{214}Po, ^{210}Pb, and Bi isotopes that are electrically charged. Thanks to this ion state they can easily attach to dust and aerosol [2] and then be inhaled and deposited inside the lung. The alpha particles produced by the decay of these isotopes are thus responsible for the internal irradiation and have a biological impact;

they deposit their energy in a small thickness of tissue, contributing significantly to the radiological dose and increasing the risk of developing lung cancer.

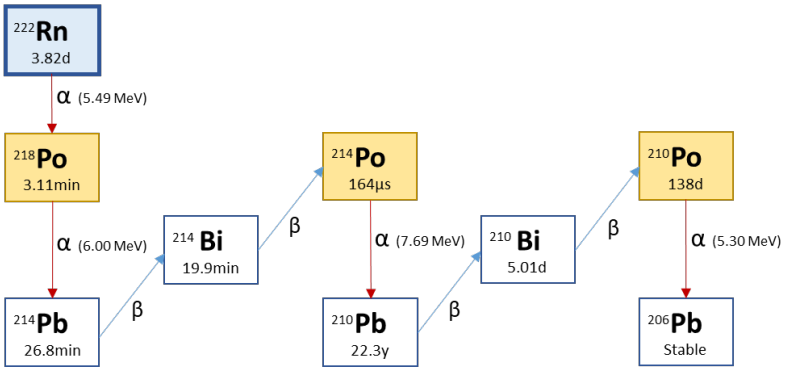

Figure 1. Part of the ^{238}U decay chain, including ^{222}Rn and its decay products (in yellow the alpha particle emitters).

In figure 1, the decay chain of ^{222}Rn is shown: its progeny are composed of Po, Bi and Pb (unstable isotopes) which are the source of alpha, beta and gamma particles. The alpha particles emitted have energies: 5.30 MeV (^{210}Po), 7.69 MeV (^{214}Po) and 6.00 MeV (^{218}Po). The alphas produced by the Polonium decays are characterized by a high ionization density with a low penetration power, maximizing the released dose and are thus responsible for the consequent biological damage. In comparison the beta particles from Bi and Pb decays release a dose that can be considered negligible. Thus the Radon with its progeny can be considered an oncogenic agent whose only effect so far is the induction of lung neoplasms [3]; it is considered the main responsible factor after cigarette smoking.

2 TPX3 detector and its main features

The TPX3 [4] is a new generation detector belonging to the family of pixel detectors developed in the context of Medipix collaboration [5]; it was developed at CERN as the successor to the Timepix1 detector [6]. It is a hybrid pixel detector, so-called because the detector is physically divided into two components: an active semiconductor sensor layer having an area 1.96 cm^2 (usually silicon or cadmium telluride) which is uniformly divided into a grid of discrete pixels (a square matrix of 256 × 256 pixels with a pitch of 55 µm) and the readout ASIC chip, based on CMOS technology. Ionizing particles interact with the semiconductor sensor material, producing primary charges (electrons or holes) that drift to the pixel producing an electronic signal. Each pixel has its own read-out circuit that provides a recording of the signal presence with its time and charge simultaneously. Coupling between sensor and chip is realized through the bump-bonding technique, and the resulting assembled sensor is mounted on a PCB board which provides additional electronic components to manage the read-out functionality. Furthermore, it is possible to adjust the detector for a specific application by varying the combination of different setting parameters. In this work, it has been fitted with the Katherine control module [7], which allows to set the TPX3 parameters and manage data acquisition (figure 2a).

2022 JINST 17 P06009

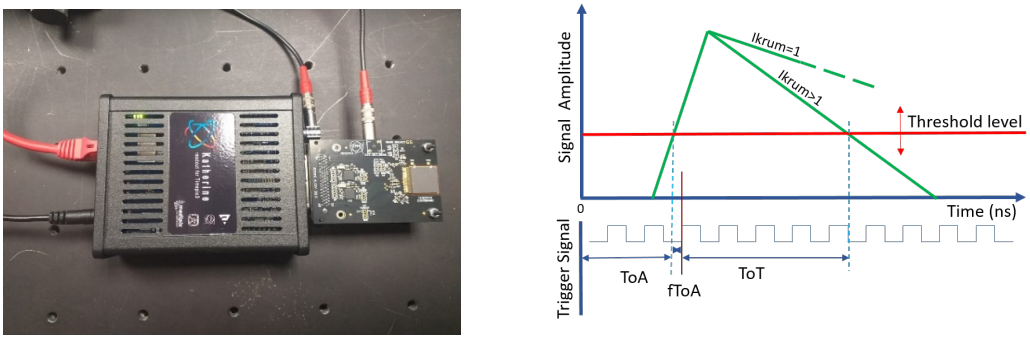

(a) (b)

Figure 2. (a): TPX3 with Katherine; (b): scheme of TPX3 acquisition modalities.

For each pixel there is a Charge Sensitive Preamplifier (CSP) that receives the current pulse induced by a particle interaction and produces an amplified output triangular signal with a longer time width (figure 2b). This signal is then compared to a threshold level and the time it is over the threshold is measured as a digital counts by a 40 MHz internal clock [8]. This is the Time over Threshold mode (ToT) and provides a digital measure of the released charge. To make better use of digitalization and improve the charge dynamic range, the CSP signal falling edge can be programmed in order to tune the pulse width. Simultaneously, the time when the rising edge of the CSP signal crosses the threshold is registered and provides the Time of Arrival (ToA) of the particle in respect to a software or hardware reference time. The maximum time resolution for ToA is 1.6 ns. TPX3 provides two acquisition modes: frame-based and data-driven. In frame-based acquisition, a fired pixel is no longer available for all the acquisition time of the frame; stored data must be first transferred at the end of the frame, and then all of the pixel matrix is ready for a new acquisition. In this configuration, registered ToA times are limited to 14 bits and cannot cover long time intervals like those set in these measurements. Then, the frame-based mode allows only a morphological and charge analysis with the possibility to manage a minor amount of data and perform a faster analysis. In data-driven mode, instead, it is no longer a sequence of frames, but a single extended time interval in which data relative to a fired pixel are immediately transferred and the pixel becomes available after a minimum of about 475 ns. In addition, the control module allows increasing the ToA range to cover longer time intervals from the measurement start. In this case, the detector is able to follow the flux of incident particles and then time stamp can be useful for a more detailed analysis, as will be shown in paragraph 3.3. At the moment two control software packages were developed, which can be used for detector parameter settings and data acquisition: Burdaman and the most recent MMtrack [9].

3 Case study: the presence of radon in NIXT laboratory and track analysis

The experimental measurements campaign was conducted at the NIXT laboratory in Frascati, a city characterized by a particular lithology. The lab rooms under study are a part of the underground workplaces and are those most affected by the radon exposure due to their location. In general, the concentration of radon in the atmosphere is governed by the intensity of the source and by dilution factors, both significantly influenced by meteorological conditions (temperature, atmospheric

2022 JINST 17 P06009

pressure, humidity, and wind conditions on the surface). In our case, the main micro-climatic parameters like relative humidity and temperature were monitored and did not show significant changes. Compared to the usual p-on-n Si Timepix, the detector used in this work is an n-on-p type CdTe TPX3: its active volume is a $14 \times 14\,mm^2$ CdTe layer having a thickness of 500 µm. It is covered by a 100 nm Al layer which works as a polarization electrode. The sensor has been biased at −150 V, the optimal observed value to assure efficient charge collection and minimize the electronic noise. The negative bias of this detector produces a localized electric field close to the Al electrode, which has the capacity to collect the positive ions coming from the decay chain of radon [10]. In addition, CdTe has a higher density with respect to Si and this increases the absorption of higher energy particles like beta electrons. The detector was positioned on an optical bench, away from heat sources, air extractors, doors, windows in order to increase the concentration of Radon and its progeny events on the sensor surface. TPX3 provides a digital reading of the released charge in ToT mode. It has been used in the frame-based mode: it acquires a sequence of frames, and each one lasts for a time width long enough to distinguish the particle tracks on the TPX3 area. In this work, the frame time width has been set to 1 s and sequences from hundreds to thousands of frames have been set to cover long times and assure an optimal statistic on the observed events. Before the operation, the detector was subjected to a procedure of threshold equalization; based only on the detector noise. The control software performs a scan of pixel threshold values with different setting parameters in order to minimize the spread of the threshold distribution. After this procedure, the minimum optimal threshold level is obtained applying a common additional value to all pixels in order to minimize the number of noisy pixels. The few ones that remains were masked, especially because they can give an unnecessary big contribution to the output data.

3.1 ToT energy calibration and spatial uniformity

The ToT acquisition mode provides a measure of the charge released pixel by pixel by interacting particles, hence an energy calibration procedure must be performed. In general, energy calibration is based on the exploitation of a given number of X-ray lines coming from radioactive sources or from X-ray fluorescence [11], but it can be calibrated in a low energy range. In this case, instead, a high energy calibration has been preferred because alphas release an amount of charge much larger than X-ray photons, thus an alpha energy scan with ^{214}Am source was used. The source was placed on a linear stage to change the alphas' energy by varying its distance with respect to the detector surface, from a minimum of 7 mm to a maximum of 37 mm with a step of 5 mm. In addition, a PVC mask with a 1 mm hole was used to select only the perpendicular outgoing alphas. A single alpha interaction switches on a cluster of pixels and the total released charge is measured by summing all the ToT pixel contributions. The result is defined as ToTvolume and is measured in clock counts (figure 3a).

According to the observed ToT distributions, a relative energy resolution between 10 and 5% for energies higher than 1.5 MeV was estimated. The experimental setup was also simulated with the Fluka MC software to estimate the energy of alphas reaching the detector. The diagram in figure 3b shows the correlation between alpha energies and the maximum ToT values. As a result, a calibration curve is obtained for high ToT values for the set acquisition parameters.

A further analysis was carried out to evaluate the detector's spatial uniformity response in ToT mode. This study was performed for different photon energies using a set of X-ray fluorescent lines

2022 JINST 17 P06009

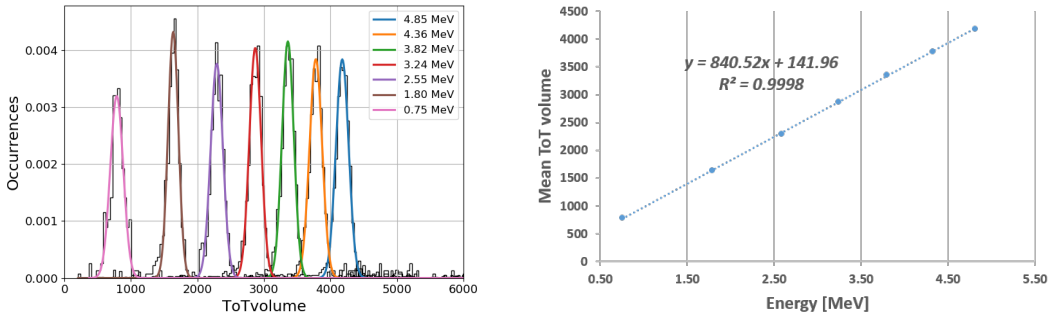

(a) (b)

Figure 3. (a): Scan in distance and response in energy (in black the experimental values, in different colors the smoothing); (b): ToT energy calibration with alphas from ^{214}Am.

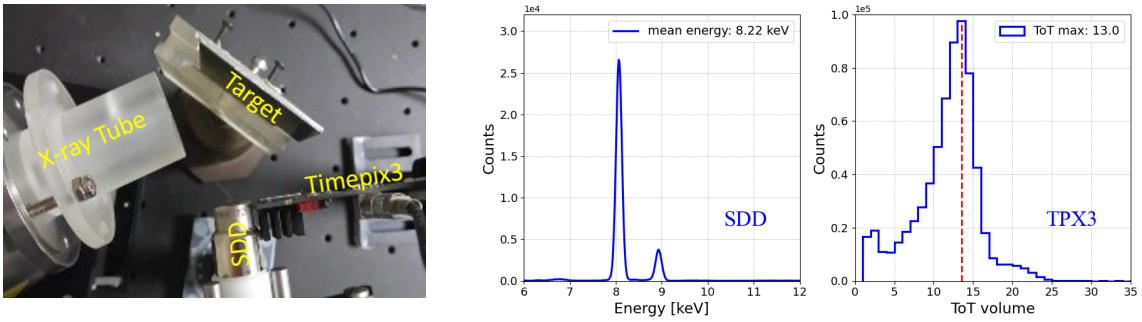

(a) (b)

Figure 4. Measurement with copper X-ray fluorescence k-lines (XRF); (a): a photo of the experimental setup with the X-ray source, target and the detectors SDD and TPX3; (b): energy spectrum measured by the SDD spectrometer in keV and TPX3 detector in ToT count units.

and irradiating all the detector area. As shown in figure 4a, the experimental set-up is composed by an X-ray source, a target, a Silicon Drift Detector (SDD) spectrometer and the TPX3.

In this case, the source was an Oxford Instrument X-ray tube working up to a maximum voltage of 50 kV and a filament current from 5 to 1000 nA. Targets of different materials (Fe, Cu, Pb, and Mo) have been used and excited through the X-ray tube. SDD spectrometer is used to verify the expected fluorescent emission lines and measure the mean photon energy for each target, while the TPX3 measures the same spectra in ToT units. Figure 4b shows the results obtained for copper. The mean energy as calculated from the measured SDD spectrum is about 8.2 keV, a weighted average between the k_α and k_β lines of copper. Simultaneously, TPX3 provides a global ToT histogram with a mean ToT value of 13 which is a measure of the mean energy of the Cu fluorescent photons interacting on the whole detector area: TPX3 has a lower energy resolution and cannot distinguish the two lines of copper. The ToT uniformity response has been evaluated by dividing all the TPX3 detector in a matrix of 4×4 sub-areas (figure 5a). Then the maximum of the ToT distribution of all the switched-on single pixels belonging to the sub-area was evaluated.

2022 JINST 17 P06009

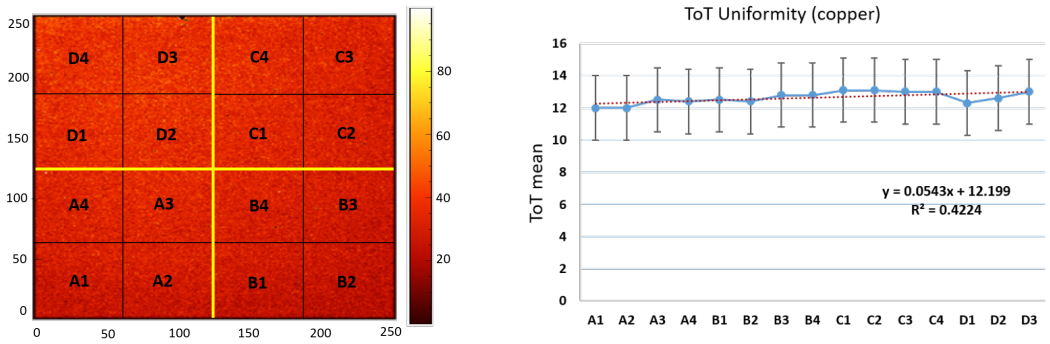

(a) (b)

Figure 5. (a): selection of clusters with size equal to 1 and maximum ToT equal to 100; (b): ToT distributions in the sixteen sub-areas.

Figure 5b shows the mean ToT and sigma values as obtained by a Gaussian fit on the ToT distributions on all the 16 sub-areas. Then, based on these results and repeating a similar analysis on the other materials, the TPX3 showed a good uniformity and the same energy calibration curve can be used for all the channels. This represents an added value in the performance characteristics of the detector itself.

3.2 Frame-based acquisition: morphological analysis

One of the objectives of this work is to characterize the response of the CdTe detector to the progeny of radon coming from the indoor air, and this response can be expressed not only in energy (and time) but also through morphological parameters. The first results of this type were obtained using the Timepix1 [2]. The 2D configuration and the high spatial resolution of the TPX3 can be exploited for morphological analysis of the particle interaction trace on CdTe. In this type of analysis the acquisitions were carried out in frame-based mode and 16 experimental runs were performed, each of 900 frames with a time width of 1 second. Depending on the type and energy of the interacting particle and the diffusion of the charge inside the CdTe, for each interaction, a cluster of pixels of a given shape will be observed (figure 6) and, for each cluster, a variety of physical, morphological parameters can be defined. The "Cluster Size" (CS) is defined as the number of adjacent pixels in a single cluster; ToT volume, as previously mentioned, is the sum of all ToT values belonging to the cluster. A 2D plot of ToT volume versus CS (figure 7a) shows at least three distinct populations: the first with low CS and low ToT volume, which is due to tracks like B and C in figure 6, the second and the third correspond to tracks A and D of the same figure.

In figure 7b for these last two populations, two peaks in ToT volume distribution can be clearly observed and, in the next section, it will be shown that they correspond to alpha decays from ^{214}Po and ^{218}Po.

In this case, these parameters are not enough to further differentiate some tracks that, from a morphological point of view, they can be easily discriminated against. To separate these tracks, a "roundness" parameter (fd_c) has been defined. It is based on the "maximum Feret's diameter", the longest distance between points around a region's convex hull contour (figure 8).

2022 JINST 17 P06009

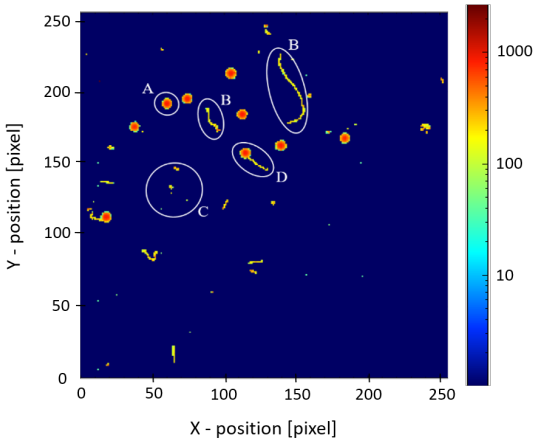

Figure 6. Tracks registered by TPX3 in a single frame: A) alpha track, B) gamma or beta track, C) soft and hard X rays, and D) complex track.

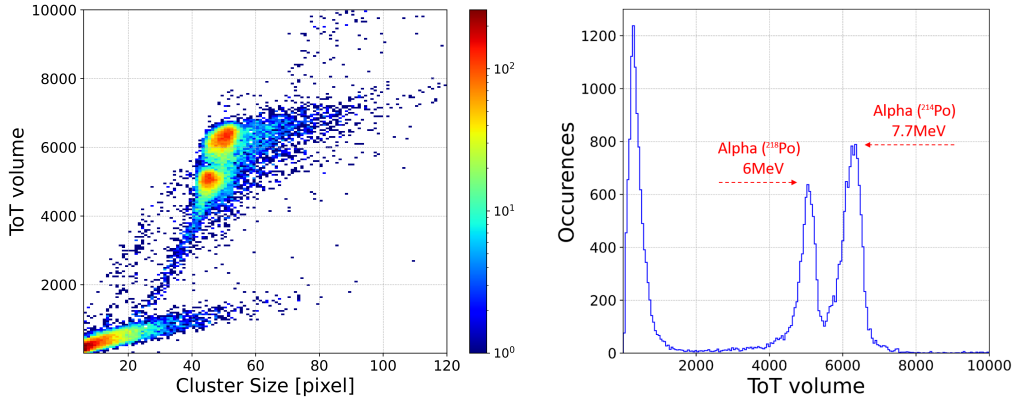

(a) (b)

Figure 7. (a) 2D plot distribution with the main particle populations: alphas from ^{214}Po and ^{218}Po have peaks in ToT volume distributions (b).

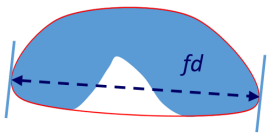

Figure 8. Maximum Feret's Diameter ($0 < f_d < 1$).

Using this geometrical concept and the CS parameter, fd_c is defined through the following formula:

$$fd_c = \frac{\sqrt{\frac{4CS}{\pi}}}{fd} \tag{3.1}$$

where the numerator defines the diameter of a circular cluster having area equal to the CS. It was

2022 JINST 17 P06009

observed that by setting $fd_c \geq 0.8$, only circular tracks are selected. This value was not determined by a particular criterion but was adjusted until clear discrimination was observed. In particular, by defining a ToT volume in a range between 10 000 and 22 000, it was observed that ToT volume distribution with $fd_c \geq 0.8$ is pratically superimposed to the distribution without cut on fd_c. Hence the majority of tracks are circular (figure 9).

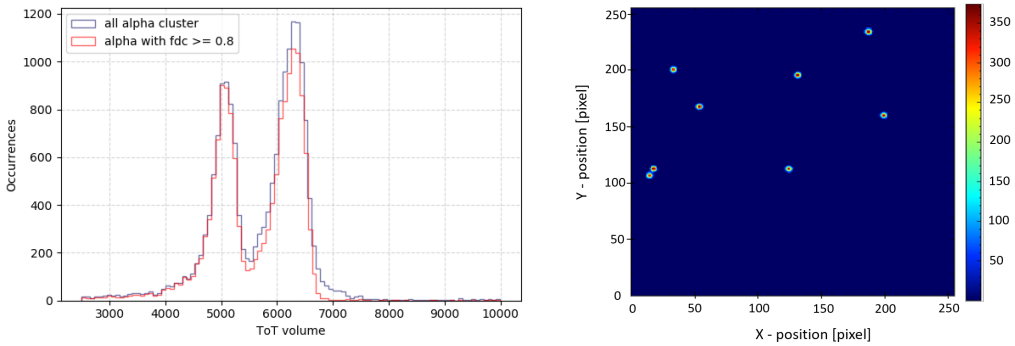

(a) (b)

Figure 9. (a) ToT distributions with the roundness morphological filter (fd_c); (b) a frame of alpha tracks belonging to the cut distribution.

3.3 Data-driven acquisition: alpha spectroscopy and temporal analysis

Similar measurements were repeated in data-driven mode. From the morphological point of view, the same results are obtained. However, in this case, tracks have been acquired with the correct timestamp, and further discrimination is possible using ToA times. Again, by defining specific cuts on CS, ToT volume and Roundness, it is possible to identify tracks coming from alpha decays in the radon chain. As shown in figure 10, the ToT volume distribution of alpha particles shows three distinct peaks. According to the calibration curve presented in figure 3b, the energies corresponding to these peaks are 5.3 ± 0.2, 5.9 ± 0.2, and 7.2 ± 0.3 MeV, and the associated errors are estimated on the FWHM of the peak distributions. The first two values are consistent with the energies of alpha particles from ^{210}Po and ^{218}Po. In this case, the presence of ^{210}Po is probably due to the long residence time of the detector in the lab, because these measures took place at least two months after those shown in the previous figure 6 and figure 9. The higher energy value is slightly underestimated with respect to the expected value of 7.69 MeV alpha energy from ^{214}Po decay. This is probably due to a trend of the calibration curve for higher energy particles as observed in Timepix1 detectors [12]. It will be further investigated in future work.

The data-driven acquisition also allows for time analysis. In particular, it has been observed that tracks with tails (like D, in figure 6) correspond to the superposition of two consecutive tracks with a time difference of a few hundreds of µs: one is a typical alpha track, the other a beta (or gamma) track, as shown in figure 11.

Then using the differences in ToA, it's possible to split the above single cluster into two clusters: one for the beta track and the other for the alpha track. Probably this is due to the beta decay of ^{214}Bi, followed by the fast alpha decay of ^{214}Po. To investigate this decay, all the couples of these

2022 JINST 17 P06009

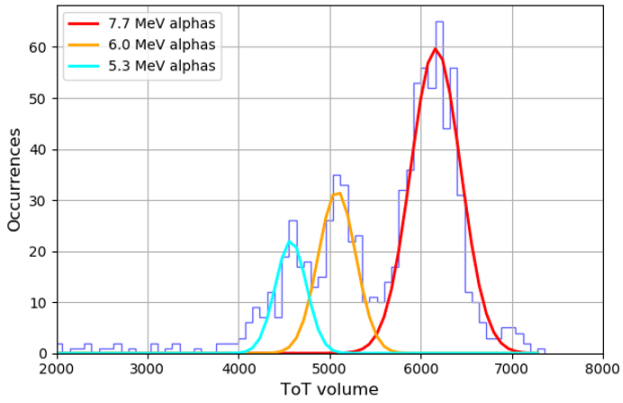

Figure 10. ToT volume distribution with the three peaks coming from alpha decays of ^{214}Po, ^{218}Po, and ^{210}Po; each peak has been fitted with a Gaussian function.

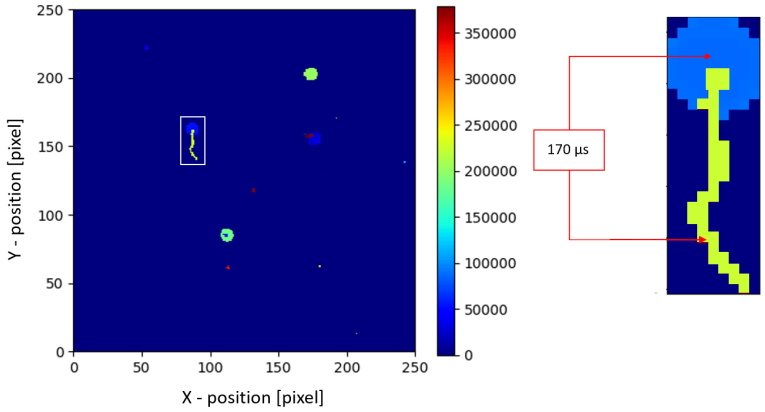

(a) (b)

Figure 11. (a) ToA matrix of a single experimental frame; (b) Zoomed-in view of the highlighted single track with "head and tail".

correlated tracks have been identified, and for each couple, the difference Δt between the mean ToA times of beta and alpha tracks has been calculated. It was then observed that the distribution of Δt follows the typical decay exponential curve with a half-life of $166 \pm 4\,\mu s$, an excellent agreement with the expected alpha decay half-life of $160\,\mu s$ from ^{214}Po (figure 12).

This demonstrates that temporal analysis can also be used effectively to further discriminate some tracks. In this case, the decay alpha half-life allows the identification of the subset of betas coming from ^{214}Bi.

4 Conclusions

The presented work highlights the performance of a CdTe TPX3 for the specific case of alpha and beta detection coming from the radon decay chain. The detector has been characterized in terms of spatial uniformity and then calibrated with alphas in a higher energy range with respect to X-rays.

2022 JINST 17 P06009

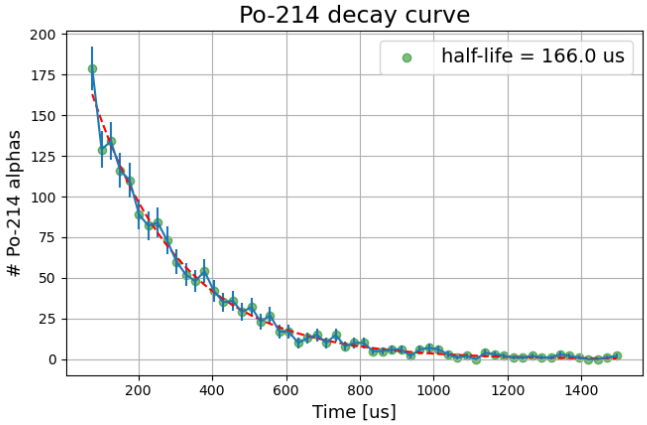

Figure 12. Half-life ^{214}Po 166 ± 4 µs; the dashed red line represents the exponential decay fit.

The potential of this detector has been demonstrated with a set of measurements on Radon decay products. A morphological cluster analysis has been presented in order to identify alpha tracks, similar to that performed with Timepix1 in previous work [2]. A significant result has been obtained from time data; it has been demonstrated that it is possible to describe the time evolution of the events coming from progeny of radon, even on very small times like it has been shown for the fast decay of ^{214}Bi isotope. Temporal analysis can be effectively applied to discriminate decay products due to particle emissions having similar energies but different half-lives. In particular this can be useful when radon, thoron and actinon are present simultaneously; in this case, in fact, radionuclides may be confused by spectrometric measurements. CdTe features combined with the functionality of the TPX3 device (high sensitivity, compactness, power off and on capability, real-time measurement, lightweight portability, high temporal resolution, high spatial and energy resolution) have demonstrated that this detector can be used for a detailed analysis of the radiation produced by radon and its progeny. The presented work can provide a new innovative method for measurements of radiation activity and dose.

Acknowledgments

The authors would like to thank P. Burian, P. Mánek and L. Meduna from the Institute of Experimental and Applied Physics in Prague for their availability to clarify and improve the new MMtrack control software. A special thank to S. Romano for discussion and suggestions and to M. Pillon providing the ^{241}Am source at the ENEA laboratory.

References

[1] *Unscear: Sources and effects of ionizing radiation*, http://digitallibrary.un.org/record/422833 [Includes bibliographical references].

[2] M. Caresana, L. Garlati, F. Murtas, S. Romano, C.T. Severino and M. Silari, *Real-time measurements of radon activity with the Timepix-based RADONLITE and RADONPIX detectors*, 2014 *JINST* **9** P11023.

2022 JINST 17 P06009

[3] H. Zeeb and F. Shannoun, eds., *WHO handbook on indoor radon: a public health perspective*, World Health Organization (2009).

[4] T. Poikela, J. Plosila, T. Westerlund, M. Campbell, M.D. Gaspari, X. Llopart et al., *Timepix3: a 65k channel hybrid pixel readout chip with simultaneous ToA/ToT and sparse readout*, 2014 *JINST* **9** C05013.

[5] *Medipix collaboration*, https://medipix.web.cern.ch 2004.

[6] X. Llopart, R. Ballabriga, M. Campbell, L. Tlustos and W. Wong, *Timepix, a 65k programmable pixel readout chip for arrival time, energy and/or photon counting measurements*, *Nucl. Instrum. Meth. A* **581** (2007) 485 [*Erratum ibid.* **585** (2008) 106].

[7] P. Burian, P. Broulím, M. Jára, V. Georgiev and B. Bergmann, *Katherine: Ethernet Embedded Readout Interface for Timepix3*, 2017 *JINST* **12** C11001.

[8] G. Claps, F. Murtas, L. Foggetta, C. Di Giulio, J. Alozy and G. Cavoto, *Diamondpix: A CVD diamond detector with timepix3 chip interface*, *IEEE Trans. Nucl. Sci.* **65** (2018) 2743.

[9] *Ieap software repository*, https://software.utef.cvut.cz (2021).

[10] F. Mamedov, P. Cermak, J. Jakubek, K. Smolek, I. Stekl and J. Vlasek, *Measurement of radon activity in air using electrostatic collection to the Timepix detector*, 2013 *JINST* **8** C03011.

[11] J. Jakubek, *Precise energy calibration of pixel detector working in time-over-threshold mode*, *Nucl. Instrum. Meth. A* **633** (2011) S262.

[12] M. Sommer, C. Granja, S. Kodaira and O. Ploc, *High-energy per-pixel calibration of timepix pixel detector with laboratory alpha source*, *Nucl. Instrum. Meth. A* **1022** (2022) 165957.

2022 JINST 17 P06009